Finite Element Analysis of Composite Sheet-Forming Processes

Conchúr M. Ó Brádaigh
R. Byron Pipes

Department of Mechanical Engineering,
University College Galway,
Galway, Ireland.

and

Center for Composite Materials,
Department of Mechanical Engineering,
University of Delaware, Newark, DE 19716, U.S.A.

To be presented at
"Flow Processes in Composite Materials",
University of Limerick, Ireland
July 4-5th, 1991

Abstract

A numerical solution technique is developed for problems of forming of highly-anisotropic composite laminates . The material is assumed to behave as a transversely isotropic Newtonian fluid, subject to the twin kinematic constraints of inextensibility in the fiber direction and material incompressibility. Assumption of plane stress conditions for thin laminae results in a simplified constitutive law, involving a single arbitrary tension stress in the reinforcement direction. The weak forms of the constraint and governing equations for creeping flow are discretized using independent interpolation of the velocity and tension stress fields. The resulting mixed system is seen to be directly analogous to the primitive variable formulation of Stokes flow. A mixed penalty finite element approach is used to solve for each step in an Updated Lagrangian solution scheme. Computations are carried out using a biquadratic velocity / bilinear discontinuous tension stress element. Solutions of flat sheet problems are presented, involving fiber orientation and element thickness updating after each time step.

1 Introduction

High performance thermoplastic composites have attracted considerable attention in recent years, not only for their improved mechanical and physical properties[1], but also because their chemistry makes rapid automated production of composite structures a possibility. Sheet-forming techniques currently in use with these materials include rubber pad forming, matched-metal die forming, hydroforming, vacuum forming and diaphragm forming[2][3][4] [5].

Sheet-forming of structural shapes from thermoplastic composites can only be viable if the results are predictable and repeatable. Numerical analysis of sheet-metal forming processes is now an essential tool for component designers, and it is likely to assume the same importance in composite processing. The aim of the current research is to develop a simulation technique which will enable the composite part designer to assess the formability of given geometries and predict finished part thickness and fiber orientation.

In composite sheet-forming, continuous[6] or aligned-discontinuous [2] fiber reinforced sheets are deformed at temperatures above the melt temperature of the polymeric matrices. The dominant characteristic of these materials is the high stiffness of the carbon fibers in comparison to that of the viscous matrix. Flow processes that occur at the polymer melt temperature are therefore highly-anisotropic, with deformations being accomodated by shearing and transverse elongational mechanisms[6] [7][8]. Methods of measuring the melt temperature viscosities of thermoplastic composites are currently being developed[9][10][11] which will provide the necessary constitutive data for numerical analysis.

Most of the predictive models being proposed for sheet forming of advanced thermoplastic composites have been purely kinematic[12][13][14]. Though useful

for predicting fiber orientation fields, these approaches do not provide the stresses and deformations at each step which would be needed to predict problems such as incomplete forming, buckling and wrinkling. Individual forming mechanisms, such as squeeze-flow[12] and interlaminar bending[15][16] have been modeled, but none of these approaches provide a basis for dealing with the forming of a complex structure. A full continuum mechanics formulation of the problem is needed in order to model the effect of parameters such as tool design, laminate shape, forming rate and ply stacking sequence on the stresses developed during forming.

An idealized theory for highly anisotropic materials has been developed [17], which treats such materials as completely inextensible in the fiber direction. This condition provides a kinematic constraint on the system, leading to simplified solutions of otherwise difficult problems. This approach has recently been extended to highly anisotropic viscous fluids[18], and has been used to obtain approximate solutions for processing problems with thermoplastic composites[19][20]. Analytical solution of these simplified flow equations for realistic forming situations can be quite difficult, even for regular shapes[21]. A numerical approach is necessary in order to deal with the geometric complexities commonly encountered in forming situations. Finite-difference schemes have been proposed for simple forming situations[22] but, as the finite element approach is is the most commonly used for complex-geometry problems, it is the chosen method in this work.

The numerical formulation presented here is a mixed penalty finite element system, which is analogous to a formulation developed by the authors for elastic problems in an earlier paper[23]. The penalty method is a popular technique for solution of mixed systems of equations, not only in finite element problems, but also in applied mathematics problems arising from constrained variational principles or the use of lagrangian multipliers [24]. The penalty method was first used in conjunction with the finite element method for solution of plate and shell problems of structural mechanics and is now an accepted technique for solution of incompressible solid and fluid mechanics problems[25][26].

2 Theoretical

2.1 Kinematics

The concept of the *Ideal Fiber Reinforced Material* was introduced by Spencer [17] for treatment of highly anisotropic elastic and plastic materials. Such a material is assumed to behave in an idealized fashion, obeying the twin constraints of inextensibility in the fiber direction and material incompressibility. These kinematic constraints restrict the range of possible deformations of the material, and are given by Rogers [18] for a fluid as:

Incompressibility

$$d_{ii} = 0 \tag{1}$$

Inextensibility in Fiber Direction

$$a_i a_j d_{ij} = 0 \tag{2}$$

where **a** is a unit vector representing the local fiber direction and **d** is the Eulerian rate-of-strain tensor:

$$d_{ij} = \frac{1}{2}\left(\frac{\partial v_i}{\partial x_j} + \frac{\partial v_j}{\partial x_i}\right) \tag{3}$$

where **v** is the velocity vector, and x_i are the components of the Cartesian axes. In general, the local fiber orientation vector is a function of both space and time.

$$\mathbf{a} = \mathbf{a}(\mathbf{x}, t) \tag{4}$$

Assuming that the fiber directions rotate as material lines during deformation, Rogers [18] gives the following expression for rotation of the local fiber orientation vector:

Fiber Rotation

$$\dot{a}_i = a_k \frac{\partial v_i}{\partial x_k} \tag{5}$$

where the superimposed dot denotes differentiation with respect to time, following a material particle, or the total time derivative.

2.2 Constitutive Theory for Newtonian Fluid

The constitutive relations for an ideal fiber-reinforced Newtonian fluid have been developed by Rogers [18]. The material is assumed to behave as a transversely isotropic linear viscous fluid, with a single family of reinforcement. Furthermore, the fibers are assumed to lie in a plane and be continuously distributed throughout, acting only as strong or preferred directions. If the fluid is incompressible and inextensible in the fiber direction, we may write the constitutive equation in indicial notation as follows:

$$\sigma_{ij} = -p\delta_{ij} + Ta_i a_j + 2\mu_T d_{ij} + 2(\mu_L - \mu_T)(a_i a_k d_{kj} + a_j a_k d_{ki}) \tag{6}$$

where δ_{ij} is the Kronecker delta, $\delta_{ij} = 1, i = j; \delta_{ij} = 0, i \neq j$, and

σ is the stress tensor.
μ_L is the longitudinal shear viscosity.
μ_T is the transverse shear viscosity.
p is an arbitrary hydrostatic pressure.
T is an arbitrary tension in the fiber direction.

The constraint equations have caused two arbitrary stress terms to appear in the constitutive equation (6). Physically, these terms are an arbitrary hydrostatic pressure (p) and an arbitrary tension stress in the fiber direction (T).
If we assume the fibers to be initially straight and parallel in a Cartesian coordinate system with axes x_1,x_2,x_3, and to lie in the 1-2 plane at an initial angle, θ to the x_1-axis, then the components of the local fiber orientation unit vector at any time instant, t become:

$$\mathbf{a} = (\cos\theta(t), \sin\theta(t), 0) \tag{7}$$

then, if we let $m = \cos\theta(t)$ and $n = \sin\theta(t)$, equation (6) may be written:

$$\begin{bmatrix} \sigma_{11} \\ \sigma_{22} \\ \sigma_{33} \\ \sigma_{23} \\ \sigma_{31} \\ \sigma_{12} \end{bmatrix} = \begin{bmatrix} D_{11} & 0 & 0 & 0 & 0 & D_{16} \\ 0 & D_{22} & 0 & 0 & 0 & D_{26} \\ 0 & 0 & D_{33} & 0 & 0 & 0 \\ 0 & 0 & 0 & D_{44} & D_{45} & 0 \\ 0 & 0 & 0 & D_{45} & D_{55} & 0 \\ D_{16} & D_{26} & 0 & 0 & 0 & D_{66} \end{bmatrix} \begin{bmatrix} d_{11} \\ d_{22} \\ d_{33} \\ 2d_{23} \\ 2d_{31} \\ 2d_{12} \end{bmatrix} + \begin{bmatrix} Tm^2 - p \\ Tn^2 - p \\ -p \\ 0 \\ 0 \\ mnT \end{bmatrix} \tag{8}$$

where, for convenience, the tensorial shear strain rates are replaced by the engineering shear strain rates, $(2d_{23}, 2d_{31}, 2d_{12})$. The terms of the viscous constitutive matrix are given as follows:

$$\begin{aligned} D_{11} &= 2\mu_T(1-2m^2) + 4\mu_L m^2 \\ D_{22} &= 2\mu_T(1-2n^2) + 4\mu_L n^2 \\ D_{33} &= 2\mu_T \\ D_{44} &= \mu_T(1-n^2) + \mu_L n^2 \\ D_{55} &= \mu_T(1-m^2) + \mu_L m^2 \\ D_{66} &= \mu_L \\ D_{45} &= (\mu_L - \mu_T)mn \\ D_{16} &= D_{26} = 2(\mu_L - \mu_T)mn \end{aligned} \tag{9}$$

The incompressibility constraint, equation (1) may be written in Cartesian coordinates as follows:

$$\frac{\partial v_1}{\partial x_1} + \frac{\partial v_2}{\partial x_2} + \frac{\partial v_3}{\partial x_3} = 0 \tag{10}$$

Similarly, the inextensibility condition, equation (2) may also be written in Cartesian coordinates:

$$\cos^2\theta(t)\frac{\partial v_1}{\partial x_1} + \cos\theta(t)\sin\theta(t)\left(\frac{\partial v_1}{\partial x_2} + \frac{\partial v_2}{\partial x_1}\right) + \sin^2\theta(t)\frac{\partial v_2}{\partial x_2} = 0 \tag{11}$$

2.3 Plane Stress in 1-2 Plane

Typical composite laminates used in the sheet-forming process are much thinner in the direction perpendicular to the plane of the fibers than in the planar directions. A reasonable assumption to employ would therefore be the existence of plane stress conditions in the 1-2 plane.

$$\sigma_{33} = \sigma_{13} = \sigma_{23} = 0 \tag{12}$$

Applying these conditions to the constitutive equations (8) and incorporating the incompressibility equation (10) leads to the following expression for hydrostatic pressure:

$$p = D_{33}d_{33} = -D_{33}(d_{11} + d_{22}) \tag{13}$$

The constitutive equation set for the ideal fluid under plane stress in the 1-2 plane is found from (13) and (8) as:

$$\begin{bmatrix} \sigma_{11} \\ \sigma_{22} \\ \sigma_{12} \end{bmatrix} = \begin{bmatrix} D_{11} + D_{33} & D_{33} & D_{16} \\ D_{33} & D_{22} + D_{33} & D_{26} \\ D_{16} & D_{26} & D_{66} \end{bmatrix} \begin{bmatrix} d_{11} \\ d_{22} \\ 2d_{12} \end{bmatrix} + \begin{bmatrix} Tm^2 \\ Tn^2 \\ mnT \end{bmatrix} \tag{14}$$

Notice that the arbitrary pressure term does not appear in this set of equations, but that the arbitrary tension in the fiber direction does. The incompressibility equation has been directly satisfied using (13). The inextensibility and fiber rotation equations (11) and (5) must still be satisfied and remain unchanged. Though the stress in the 3-direction has been set to zero, the strain rate has not, and may be found, after solution for the velocity field, by using (1).

2.4 Updated Lagrangian Scheme

The following assumptions are employed in order to obtain a numerical solution for composite sheet-forming problems:

1. Acceleration effects are neglected. This is a reasonable assumption as most sheet-forming processes are carried out over a period of minutes rather than seconds.

2. Variables are referred to a material set of coordinates (denoted X_1, X_2, X_3), where the coordinate frame follows the material points during deformation.

3. The time domain is divided into a number of increments, in each of which steady-state conditions exist.

4. The deformation during each time step is assumed to be small.

The problem is divided into a series of independent problem in a quasi steady-state fashion. Following the solution for a single time step, the configuration and properties of the body are updated and used as input for the next time step. This approach is known as the Updated Lagrangian Scheme [27].

For an isolated volume of fluid at an instant in time, the equilibrium and boundary traction equations are given as:

$$\sigma_{ij,j} + b_i = 0 \text{ in } \Omega \tag{15}$$

$$\bar{t}_j = n_i \sigma_{ij} \text{ on } \Gamma_t \tag{16}$$

where Ω is the problem domain, Γ_t is the boundary on which the tractions $\mathbf{t}$ are prescribed, and n_i are the components of the unit normal vector to the boundary. b_i are the components of the constant body forces, such as gravity.

In the Lagrangian description, the finite deformation rate tensor, $\mathbf{d}$ has both first-order and second-order terms [28]:

$$d_{ij} = \frac{1}{2}\left(\frac{\partial v_i}{\partial X_j} + \frac{\partial v_j}{\partial X_i} + \frac{\partial v_k}{\partial X_i}\frac{\partial v_k}{\partial X_j}\right) \tag{17}$$

The assumption that the deformations are small, $(\partial v_i / \partial X_j \ll 1)$ leads to the infinitesmal deformation rate tensor:

$$d_{ij} = \frac{1}{2}\left(\frac{\partial v_i}{\partial x_j} + \frac{\partial v_j}{\partial x_i}\right) \tag{18}$$

where the lower case letters x_1, x_2, x_3 are used to denote the small-deformation formulation.

The fiber rotation equation (5) is expanded for Lagrangian coordinates as:

$$\frac{\partial a_i}{\partial t} = a_k \frac{\partial v_i}{\partial X_k} \tag{19}$$

During each time increment the steady-state assumption therefore precludes any change in fiber orientation. However, the orientation is updated after each time step $(\Delta t)_n$ as follows:

$$\textit{for time step } n\textit{:}\ (a_i)_{n+1} = (a_i)_n + (\Delta a_i)_n = (a_i)_n + (\Delta t)_n \left(a_k \frac{\partial v_i}{\partial x_k}\right)_n \tag{20}$$

Thus, for quasi-steady state conditions, the appropriate equation to update the fiber orientation field angle, $\theta(x_1, x_2)$, for a time increment, $(\Delta t)_n$ can be written in Cartesan coordinates as:

$$\theta(x_1, x_2)_{n+1} = \theta(x_1, x_2)_n + (\Delta t)_n \left\{\frac{\partial v_2}{\partial x_1} + \tan\theta(x_1, x_2)\frac{\partial v_2}{\partial x_2}\right\}_n \tag{21}$$

In a similar fashion, the updated body configuration can be found after each time step from the velocity field:

$$(x_1, x_2, x_3)_{n+1} = (x_1, x_2, x_3)_n + (\Delta t)_n (v_1, v_2, v_3)_n \tag{22}$$

The solution procedure may be summarized as follows:

- Step 1 The boundary value problem described by equations (18), (15), (16), and (14) is solved for each time step $(\Delta t)_n$. Solution variables include velocity, stress and strain rate fields.
- Step 2 The body configuration is updated from the velocity field using equation (22).
- Step 3 The fiber orientation field is updated using equation (21). The terms of the constitutive matrix (9) are then updated to ake account of changed fiber orientation.
- Step 4 The boundary value problem for the next time step $(\Delta t)_{n+1}$ is solved on the updated configuration.

3 Finite Element Formulation

3.1 Weak Formulation

The weak form of the equilibrium equations is found by introducing an arbitrary velocity vector, $\delta\mathbf{v}$, and summing the work done on the body. The equilibrium equations (15) are premultiplied by the components of the arbitrary velocity vector (for plane stress in the 1-2 plane) and integrated over the problem domain, Ω as follows:

$$\int_\Omega \{\delta v_1(\frac{\partial \sigma_{11}}{\partial x_1} + \frac{\partial \sigma_{12}}{\partial x_2} + b_1) + \delta v_2(\frac{\partial \sigma_{21}}{\partial x_1} + \frac{\partial \sigma_{22}}{\partial x_2} + b_2)\} d\Omega = 0 \tag{23}$$

Integrating by parts and employing Green's Theorem leads to the *virtual work equation*:

$$\int_\Omega \delta\dot{\epsilon}^T \sigma d\Omega - \int_\Omega \delta\mathbf{v}^T \mathbf{b} d\Omega - \int_\Gamma \delta\mathbf{v}^T \bar{\mathbf{t}} d\Gamma = 0 \tag{24}$$

where the six stress components σ, and the six components of the virtual strain rate vector, $\delta\dot{\epsilon}$ have been arranged in column matrices. The virtual strain rate is defined as:

$$\delta\dot{\epsilon} = \mathbf{S}\delta\mathbf{v} \tag{25}$$

where $\mathbf{S}$ is the plane stress derivative operator matrix.

The constitutive equation (8 is first re-written as follows:

$$\sigma = \mathbf{D}\dot{\epsilon} + \mathbf{a}T \tag{26}$$

where $\mathbf{a}^T$ is given as

$$\mathbf{a}^T = \begin{bmatrix} \cos^2\theta & \sin^2\theta & \cos\theta\sin\theta \end{bmatrix} \tag{27}$$

and then substituted into the virtual work equation (24):

$$\int_\Omega \delta\dot{\epsilon}^T \mathbf{D}\epsilon d\Omega + \int_\Omega \delta\dot{\epsilon}^T \mathbf{a} T d\Omega - \int_\Omega \delta\mathbf{v}^T \mathbf{b} d\Omega - \int_\Gamma \delta\mathbf{v}^T \bar{\mathbf{t}} d\Gamma = 0 \tag{28}$$

Equation (28) above represents the weak form of the equilibrium equations, incorporating the constitutive equations. The remaining equation is the inextensibility constraint in the fiber direction.

In developing the weak form of the inextensibility condition, equation (11), notice that the equation may be recast in matrix form as:

$$\mathbf{a}^T \mathbf{S}\mathbf{v} = 0 \tag{29}$$

Introducing an arbitrary weighting function, $(\delta T)^T$, premultiplying equation (29) and integrating for fiber inextensibility over the entire domain, results in

$$\int_\Omega (\delta T)^T \mathbf{a}^T \mathbf{S}\mathbf{v} d\Omega = 0 \tag{30}$$

3.2 Discretization

The governing integral equations of the problem (28) and (30) are to be discretized at nodes distributed throughout the domain, by the use of suitable interpolation functions. In this case the solution parameters at each node are the velocity vector $\mathbf{v}$ and the scalar tension stress in the fiber direction. The velocity and tension fields will be discretized independently, employing two sets of interpolation functions as follows:

$$\mathbf{v} \approx \hat{\mathbf{v}} = \mathbf{N}^v \mathbf{a}^v \; ; \; T \approx \hat{T} = \mathbf{N}^t \mathbf{a}^t \tag{31}$$

where $\mathbf{N}^v$ and $\mathbf{N}^t$ are the velocity and tension interpolation functions, and $\mathbf{a}^v$ and $\mathbf{a}^t$ are the listings of nodal velocities and tensions. Applying the above interpolations to the virtual velocity and strain rate terms of equation (28):

$$\delta\mathbf{v} = \mathbf{N}^v \delta\mathbf{a}^v \text{ and } \delta\dot{\epsilon} = \mathbf{S}\mathbf{N}^v \delta\mathbf{a}^v = \mathbf{B}^v \delta\mathbf{a}^v \tag{32}$$

Inserting these relationships into the virtual work equation (28), we find:

$$(\delta\mathbf{a}^v)^T \{ \int_\Omega (\mathbf{B}^v)^T \mathbf{D}\mathbf{B}^v \mathbf{a}^v d\Omega + \int_\Omega (\mathbf{B}^v)^T \mathbf{a}\mathbf{N}^t \mathbf{a}^t d\Omega$$
$$- \int_\Omega (\mathbf{N}^v)^T \mathbf{b} d\Omega - \int_\Gamma (\mathbf{N}^v)^T \bar{\mathbf{t}} d\Gamma \} = 0 \tag{33}$$

The weak form of the inextensibility equation is found by substituting (31) and (32) into equation (30):

$$(\delta\mathbf{a}^t)^T \int_\Omega (\mathbf{N}^t)^T \mathbf{a}^T \mathbf{B}^v \mathbf{a}^v d\Omega = 0 \tag{34}$$

Noting that the identities in equations (33), and (34) must be true for all variations of the arbitrary parameters $\delta \mathbf{a}^v$ and $\delta \mathbf{a}^t$, the complete equation system may be summarized as follows:

$$\begin{bmatrix} \mathbf{K} & \mathbf{K}^t \\ (\mathbf{K}^t)^T & 0 \end{bmatrix} \begin{bmatrix} \mathbf{a}^v \\ \mathbf{a}^t \end{bmatrix} + \begin{bmatrix} \mathbf{f} \\ 0 \end{bmatrix} = 0 \tag{35}$$

For any two nodes i and j, the matrix components are given by:

$$\mathbf{K}_{ij} = \int_\Omega (\mathbf{B}_i^v)^T \mathbf{D} \mathbf{B}_j^v d\Omega$$

$$\mathbf{K}_{ij}^t = \int_\Omega (\mathbf{B}_i^v)^T \mathbf{a} \mathbf{N}_j^t d\Omega$$

$$\text{and} \quad \mathbf{f} = -\int_\Omega (\mathbf{N}_i^v)^T \mathbf{b}_0 d\Omega - \int_\Gamma (\mathbf{N}_i^v)^T \bar{\mathbf{t}} d\Gamma \tag{36}$$

where the system unknowns $\mathbf{a}^v$ and $\mathbf{a}^t$ represent the nodal velocities and tensions. This plane stress system will be known as the *v-T formulation*. We note that whereas the first derivative of the velocity shape functions $\mathbf{B}^v$ is involved, no derivative of the tension stress functions $\mathbf{N}^t$ appears, and they may therefore be discontinuous between elements.

A direct analogy exists between the primitive variable formulation for an isotropic incompressible fluid[29] and the plane stress formulation for a similar fluid reinforced with inextensible fibers[3][23]. In both cases the velocity is the primary variable. The secondary or constraint variable is an arbitrary stress, in one case a hydrostatic pressure, in the other a tension stress in the fiber direction.

3.3 Mixed Penalty Formulation

Implementation of penalty formulations in problems of incompressible elasticity and flow, such as the Navier-Stokes equations, has taken two forms, one irreducible [30], the other a mixed technique [31]. By analogy with Stokes flow [31] [32], we may write a mixed penalty formulation for the current problem, the first step being the construction of an approximation for the tension field, as follows:

$$T = \alpha \mathbf{a}^T \epsilon = \alpha \mathbf{a}^T \mathbf{S} \mathbf{v} \ ; \text{ as } \alpha \to \infty \tag{37}$$

Discretization of equation (37) is followed by substitution into (35), leading to the following penalized system:

$$\begin{bmatrix} \mathbf{K} & \mathbf{K}^t \\ (\mathbf{K}^t)^T & -\frac{1}{\alpha}\mathbf{M}^t \end{bmatrix} \begin{bmatrix} \mathbf{a}^v \\ \mathbf{a}^t \end{bmatrix} + \begin{bmatrix} \mathbf{f} \\ 0 \end{bmatrix} = 0 \ ; \text{ as } \alpha \to \infty \tag{38}$$

where $\mathbf{M}^t$ correlates exactly with the pressure mass-matrix for Stokes flow [31], and will thus be known as the *tension mass-matrix*, defined as follows:

$$\mathbf{M}_{ij}^t = \int_\Omega \mathbf{N}_i^t \mathbf{N}_j^t d\Omega \tag{39}$$

As the tension field may be discontinuous between elements, $\mathbf{a}^t$ is eliminated, yielding

$$\{\mathbf{K} + \alpha \mathbf{K}^t (\mathbf{M}^t)^{-1} (\mathbf{K}^t)^T\} \mathbf{a}^v = \mathbf{f} \tag{40}$$

As the penalty number α tends to infinity, satisfaction of the inextensibility constraint is achieved.

Even though the only solution parameters remaining in the penalized system (40) are the velocity unknowns, $\mathbf{a}^v$, the system is still a mixed system, as the tension constraint matrix $\mathbf{K}^t$ contains both velocity and tension shape function terms (36). For this reason, this method is known as the *mixed* or *consistent penalty method*.

After solution of the velocity field from (40), the tension field may be recovered, as follows:

$$\mathbf{a}^t = \alpha (\mathbf{M}^t)^{-1} (\mathbf{K}^t)^T \mathbf{a}^v \tag{41}$$

4 Results

4.1 Computational

A specialised finite element program has been developed[3] for composite sheet-forming problems, using the mixed penalty formulation of equation (40). The program, known as FEFORM, is based on a general purpose finite element code called PCFEAP [25], which was made available by the University of California at Berkeley. The FEFORM code runs on a VAX 11/785 minicomputer, and uses double precision throughout. For more details on the element and program construction, the reader should consult references[3] and[23].

The element used in this work utilizes biquadratic velocity interpolation functions, combined with bilinear tension stress functions. This element is known as the Q 9/4 element and is shown in Figure 1 to have 9 velocity nodes and 4 internal tension stress nodes. The inputs to the program include the mesh and node location, the initial sheet dimensions, thickness and fiber orientation, the material viscosities μ_L and μ_T, the total time and number of time increments and finally, the loading and boundary conditions.

The element matrices, $\mathbf{K}$, $\mathbf{K}^t$ and $\mathbf{M}^t$ are evaluated using a 3×3 Gaussian integration scheme and the system equations (40) solved for the velocity unknowns at each step. The total stress is then evaluated using equation (26), with the extra stress and reaction stress terms both being extrapolated to the velocity nodes before being added together. Further details on the stress calculations and fiber orientation and sheet thickness updating procedures are contained in reference[3].

The results in the next section were obtained by executing the program on a VAX 11/785 minicomputer. As the equation system is linear, no special solution technique is required, the only extra effort compared to problems of Stokes flow being the evaluation of the constraint matrices. The formulation is not, therefore,

very c.p.u. intensive, varying from about 33 seconds c.p.u. time per time step for a 24 element mesh to about 3 minutes per time step for the 192 element mesh used in the following examples. The user must ensure that the time step is small enough to maintain the small-deformation assumption at each step, within certain realistic economic bounds.

4.2 Examples

A previous paper[23] presented results for the analogous highly-anisotropic linear elastic formulation. The Q 9/4 element was shown to give acceptable displacement and stress results, with extensions in the fiber direction converging to machine zero for a penalty number of 10^{16}. The results were shown to compare well to closed-form solutions for the simple case of the 0° beam and highlighted the existence of extremely thin boundary layers of high stresses in these materials. Rather than repeat these results, this section will concentrate on the deformed states and updated fiber orientations after various time steps. All results shown are obtained utilizing a penalty number of 10^{15} and typical APC-2 viscosities[6][11] of $\mu_L = 6000$ N.s/m^2 and $\mu_T = 3500$ N.s/m^2.

The 192 element mesh used is shown in Figure 2, with built-in boundary conditions at one end and either uniform shear or tensile loading applied to the other end. Figure 3(a) shows a tensile loading being applied to a beam with 0° fiber orientation (depicted by the arrows) for a total time of 15 seconds, using a time step of 0.5 seconds. After 2 seconds, the deformed geometry, shown in Figure 3(b) resembles the classical first time step results of simple shear deformation[23], though in this case, the fibers clearly follow the deformation. Figures 3(c)-(e) show the deformations and updated orientations after 5,10, and 15 seconds. All the deformed geometries are shown to scale, thus we can clearly see that the inextensibility condition forces the edge originally at $x = 0.32$ to move inwards. At the later times, 10 and 15 seconds, we also see some curvature starting to occur in the beam, near the built-in edge.

The reason for this curvature is seen in the contour plots of updated thickness in Figures 5 and 6. The through-the-thickness strain-rate, which governs any change in thickness is dependent on the 1 and 2 normal strain-rates. In this case, as the fibers lie in the x-direction, the 1-strain rate will be zero. The 2-strain rate is dependent on the variation of the y-velocity, v in the y-direction. In plane-strain cases[33] it may be shown that the dual constraints of incompressibility and fiber inextensibility dictate that the velocity, v may not vary in the y-direction. However, in our case the plane stress elements do not enforce incompressibility in the plane but rather update their thicknesses after each time step to conserve volume. This explains the variation in thickness after 5 seconds, seen in Figure 5. This variation in thickness of +2% and -1% causes a gradient in element properties, which in turn causes the curvature near the built-in end at later times. The thickness contours at fifteen seconds, shown in Figure 6 show an even

more pronounced variation in thickness, from +15% and -4%. It should be noted that fiber orientation changes and thickness changes are cumulative, even though they are calculated by using the current values of strain rates at the end of each time step.

A second example of this updated geometry and material properties is that of tension applied to the end of a 90° beam. The original mesh is shown in Figure 7(a) and deformed meshes after 5 and 15 seconds in Figures 7(b) and 7(c). The remarkable aspect of these solutions is that the inextensibility of the fibers in the y-direction precludes any change in y-dimension of the beam as it elongates. The increase in beam area in the plane is accompanied by a uniform decrease of beam thickness throughout. Finally, we note that the fibers do not rotate, as there is no shear strain term to cause rotation.

Finally, we present the updated solutions for a tensile stress applied to the end of a 45° beam. The original mesh and fiber orientation is shown in Figure 8(a) and the deformed mesh at 5 seconds in Figure 8(b). Again, we see a curvature effect near the built-in end, which becomes more pronounced in Figure 8(c) as the beam continues to be extended at 15 seconds. It is possible to present the rotated fiber directions as arrows but it is perhaps more instructive, in this case. to show the same information in the form of contour plots, as depicted in Figures 9 and 10. Fiber rotation varies from 42.3° to 37.0° at 5 seconds, and from 38.8° to 23.6° at 15 seconds. Finally, the thickness contours for 5 and 15 seconds are shown in Figures 11 and 12. The thickness decreases everywhere at each time step, with the maximum thickening occurring at the $x = 0, y = 0.16$ top left hand corner. This makes sense, as most extension occurs perpendicular to the +45° direction. After 15 seconds, the thickness change varies from -9.3% to -17.7%.

5 Conclusions

A finite element methodology has ben demonstrated for analysis of composite materials sheet-forming problems. An Updated Lagrangian solution scheme has been adopted to describe the deformation of the material, involving dimensional and fiber orientation field changes after each time step. The formulation incorporated the highly anisotropic nature of these materials by introducing the kinematic constraint of inextensibility in the fiber direction. The plane stress case studied led to a mixed system of equations, directly analogous to those of Stokes flow, amenable to solution by penalty methods.

The FEFORM finite element code was seen to have the capability to deal with the concepts of changing fiber orientation and thickness field as the with progressing deformation. A number of simple beam examples were demonstrated involving significant changes in both thickness and orientation. The results illustrated the non-intuitive nature of deformations of highly-anisotropic materials and showed the potential of this approach for simulation of composite sheet-

forming processes. At present the program is limited to problems of plane stress only, but it is hoped to extend the capabilities to deal with curvilinear shell-type structures in the future.

6 Acknowledgements

The authors would like to thank Imperial Chemical Industries PLC, who supported this work through a Composite Sheet Forming Graduate Fellowship. We would also like to acknowledge Professor R. L. Taylor of the University of California at Berkeley, for the use of the PCFEAP code.

References

[1] National Materials Advisory Board. The Place for Thermoplastic Composites in Structural Composites. Technical Report 434, National Research Council, 1987.

[2] R.K. Okine. Analysis of Forming Parts from Advanced Thermoplastic Composite Sheet Materials. *Journal of Thermoplastic Composite Materials*, 2(1):50–76, January 1989.

[3] C.M. Ó Brádaigh. *Analysis and Experiments in Diaphragm Forming of Continuous Fiber Reinforced Thermoplastics.* PhD thesis, Department of Mechanical Engineering, University of Delaware, December 1990.

[4] C.M. Ó Brádaigh, R.B. Pipes, and P.J. Mallon. Issues in Diaphragm Forming of Advanced Thermoplastic Composites. *Polymer Composites*, 1991. in press.

[5] P.J. Mallon, C.M. Ó Brádaigh, and R.B. Pipes. Polymeric Diaphragm Forming of Complex-Curvature Thermoplastic Composites. *Composites*, 20(1):45–56, January 1989.

[6] F.N. Cogswell. The Processing Science of Thermoplastic Structural Composites. *International Polymer Processing*, 1(4):157–165, 1987.

[7] J.A. Barnes and F.N. Cogswell. Transverse Flow Processes in Continuous Fibre-Reinforced Thermoplastic Composites. *Composites*, 20:38–42, 1989.

[8] C.M. Ó Brádaigh and P.J. Mallon. Effect of Forming Temperature on the Properties of Polymeric Diaphragm Formed Thermoplastic Composites. *Composite Science and Technology*, 35(1):235–255, July 1989.

[9] P.V. Kaprelian and T.G. Rogers. Determination of the Shear Modulii of Fibre-Reinforced materials by Centred and Off-Centred Torsion. In *Proceedings of the 34th SAMPE International Symposium*, May 1989. Reno, Nevada.

[10] D.J. Groves. A Characterisation of Shear-Flow in Continuous Fibre Thermoplastic Laminates. *Composites*, 20(1):28–32, January 1989.

[11] J.J. Scobbo and N. Nakajima. Dynamic Mechanical Analysis of Molten Thermoplastic / Continuous Graphite Fiber Composites in Simple Shear Deformation. In *Proceedings of the 21st International SAMPE Technical Conference*, September 1989. Atlantic City, New Jersey.

[12] A.J. Smiley. *Diaphragm Forming of Carbon Fiber Reinforced Thermoplastics.* PhD thesis, Department of Mechanical Engineering, University of Delaware, May 1988.

[13] B.P. VanWest. *A Simulation of the Draping and a Model of the Consolidation of Commingled Fabrics.* PhD thesis, Department of Mechanical Engineering, University of Delaware, May 1990.

[14] A.S. Tam and T.G. Gutowski. The Kinematics for Forming Ideal Aligned Fiber Composites Into Complex Shapes. *Composites Manufacturing*, 1990. submitted.

[15] A.S. Tam and T.G. Gutowski. Ply-Slip During the Forming of Thermoplastic Composite Parts. *Journal of Composite Materials*, 23:587–605, 1989.

[16] M.F. Talbot and A.K. Miller. A Model for Laminate Bending under Arbitrary Curvature Distribution and Extensive Interlaminar Sliding. In *Winter Annual Meeting of the American Society of Mechanical Engineers, Symposium on Processing of Polymers and Polymer Composites*, December 1989. San Francisco.

[17] A.J.M. Spencer. *Deformations of Fibre Reinforced Materials.* Clarendon Press, Oxford, 1972.

[18] T.G. Rogers. Rheological Characterisation of Anisotropic Materials. *Composites*, 20(1):21–27, January 1989.

[19] R. Balasubramanyam, R.S. Jones, and A.B. Wheeler. Modelling Transverse Flows of Reinforced Thermoplastic Materials. *Composites*, 20(1):33–37, January 1989.

[20] P.V. Kaprelian and J.M. O'Neill. Shearing Flow of Highly Anisotropic Laminated Composites. *Composites*, 20(1):43–47, January 1989.

[21] J.M. O'Neill. The Forming of Fibre-Reinforced Composites (Part 1). ICI Joint Research Scheme, Paper No.1/89, April 1989.

[22] J.M. O'Neill. The Forming of Fibre-Reinforced Composites (Part 2). ICI Joint Research Scheme, Paper No.2/89, July 1989.

[23] C.M. Ó Brádaigh and R.B. Pipes. A Finite Element Formulation for Highly Anisotropic Incompressible Elastic Solids. *International Journal for Numerical Methods in Engineering*, 1991. in press.

[24] M. Fortin and R. Glowinski. *Augmented Lagrangian Methods: Applications to the Numerical Solution of Boundary-Value Problems*, volume No. 15 of *Studies in Mathematics and its Applications*. North-Holland, New York, 1983.

[25] O.C. Zienkiewicz and R.L. Taylor. *The Finite Element Method*, volume 1. McGraw-Hill, London, fourth edition, 1989.

[26] G. Dhatt and G. Hubert. A Study of Penalty Elements for Incompressible Laminar Flows. *International Journal for Numerical Methods in Fluids*, 6:1–19, 1986.

[27] Lawrence E. Malvern. *Introduction to the Mechanics of a Continuous Medium*. Prentice-Hall, New Jersey, 1969.

[28] W.M. Lai, D. Rubin, and E. Krempl. *An Introduction to Continuum Mechanics*. Pergamon Press, Oxford, revised edition, 1978.

[29] C. Taylor and P. Hood. A Numerical Solution of the Navier-Stokes Equations using the Finite Element Method. *Computers and Fluids*, 1:73–100, 1973.

[30] J.T. Oden. RIP Methods for Stokesian Flows. In R.H. Gallagher, D.H. Norrie, J.T. Oden, and O.C. Zienkiewicz, editors, *Finite Elements in Fluids*, chapter 15, pages 305–318. John Wiley and Sons, New York, 1982.

[31] M.S. Engelman, R.L. Sani, P.M. Gresho, and M. Bercovier. Consistent Vs. Reduced Integration Penalty Methods for Incompressible Media Using Several Old and New Elements. *International Journal for Numerical Methods in Fluids*, 2:25–42, 1982.

[32] M. Fortin. Two Comments on: Consistent Vs. Reduced Integration Penalty Methods for Incompressible Media Using Several Old and New Elements. *International Journal for Numerical Methods in Fluids*, 3:93–98, 1983.

[33] A.C. Pipkin and T.G. Rogers. Plane Deformations of Incompressible Fiber-Reinforced Materials. *Journal of Applied Mechanics*, 38:634–640, 1971.

7 Appendix: Notation

$\mathbf{a}$ Fiber orientation vector.

$\mathbf{a}^v$ List of nodal velocities.

$\mathbf{a}^p$ List of nodal pressures.

$\mathbf{a}^t$ List of nodal tensions.

α Penalty number.

$\mathbf{b}$ Body force vector.

$\mathbf{B}^v$ Velocity shape function derivative matrix.

$\mathbf{C}^t$ Consistent penalty constraint matrix.

$\mathbf{d}$ Deformation rate tensor.

$\mathbf{D}$ Constitutive matrix.

δ Kronecker delta function.

$(\Delta\mathbf{a})_n$ Incremental change in fiber orientation vector during nth time step.

$(\Delta t)_n$ nth time step.

$\dot{\epsilon}$ Strain rate vector.

$\delta\dot{\epsilon}$ Virtual strain rate vector

$\mathbf{f}$ Residual (right-hand side) vector.

Γ_t Traction boundary.

$\mathbf{K}$ Stiffness matrix.

$\mathbf{K}^t$ Tension constraint matrix.

$\mathbf{K}^p$ Pressure constraint matrix.

$\mathbf{M}$ Tension mass-matrix.

m Cosine θ.

μ_L Longitudinal shear viscosity.

μ_T Transverse shear viscosity.

n Sine θ.

$\mathbf{n}$ Unit normal to boundary.

n_v Number of velocity unknowns in element.

n_t Number of tension unknowns in element.

$\mathbf{N}^v$ Velocity shape function vector.

$\mathbf{N}^t$ Tension shape function vector.

Ω Problem domain.

p Arbitrary hydrostatic pressure.

$\mathbf{Q}$ Matrix used to construct stiffness matrix.

$\mathbf{S}$ Partial derivative matrix.

σ Stress tensor.

T Arbitrary tension stress.

$\hat{T}$ Discretized tension stress.

$\bar{\mathbf{t}}$ Traction vector.

θ Fiber orientation angle.

$\mathbf{v}$ Velocity vector.

$\delta\mathbf{v}$ Virtual velocity vector.

$\hat{\mathbf{v}}$ Discretized velocity vector.

V Volume of domain.

x_i Components of Eulerian axes.

X_i Components of Lagrangian axes.

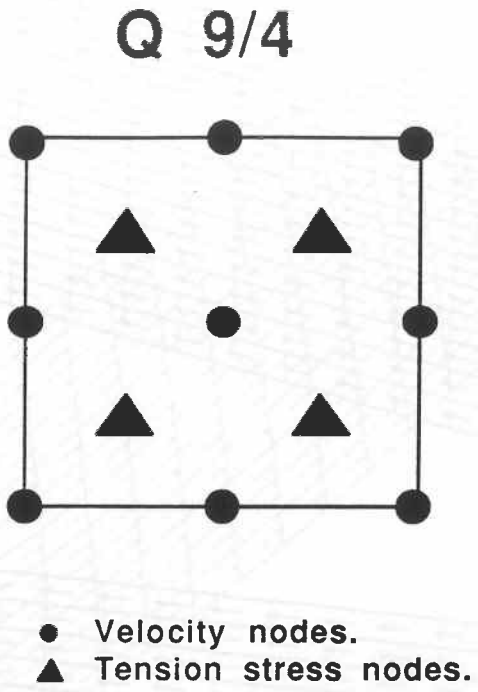

Figure 1: Q 9/4 Biquadratic Velocity / Bilinear Discontinuous Tension Stress Element

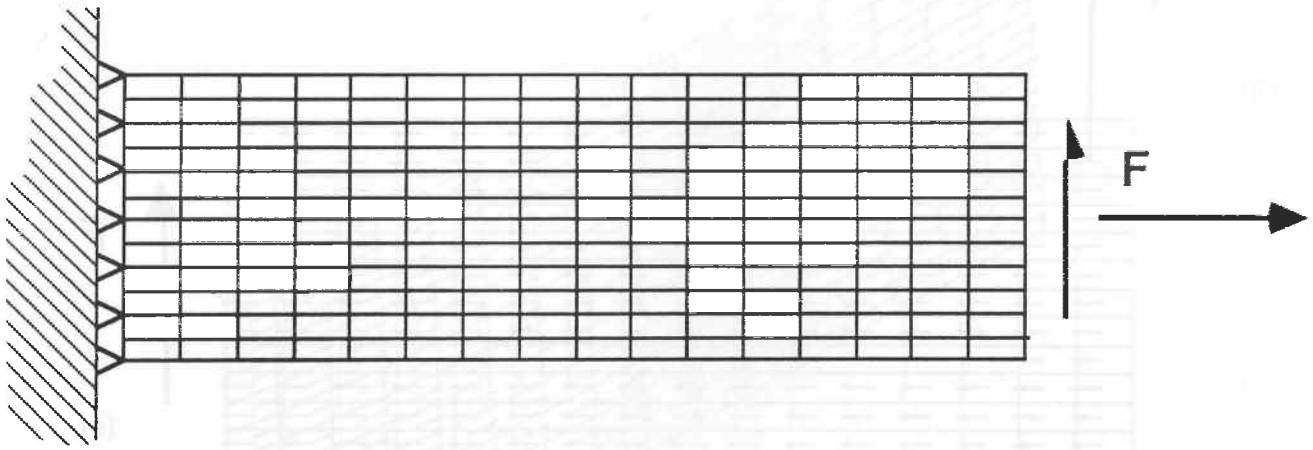

Figure 2: Loading Cases 1 & 2: Uniform Tensile and Shear Loads Applied to Beam End.

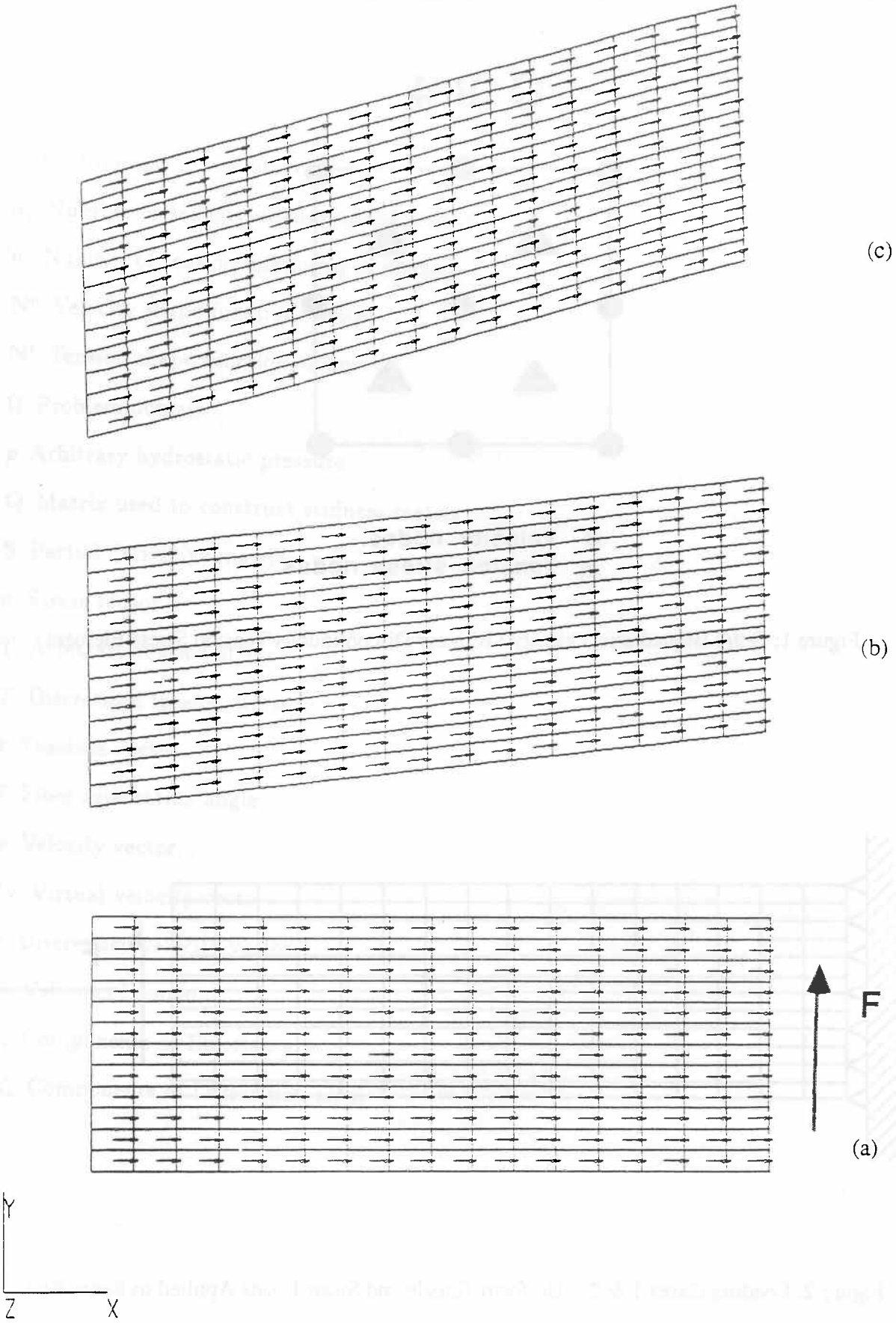

Figure 3: Cantilever Beam (a) shown in original position.
(b) Updated Geometry and Fiber Orientation After 2 seconds, 4 Time Steps,
(c) Updated Geometry and Fiber Orientation After 5 seconds, 10 Time Steps.

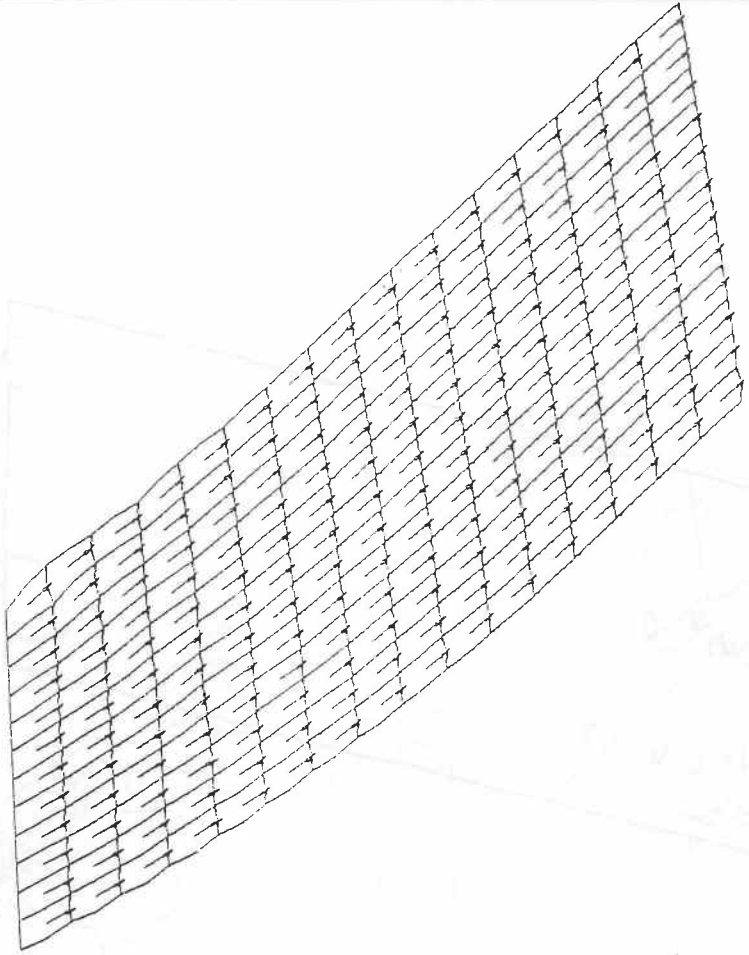

(e)

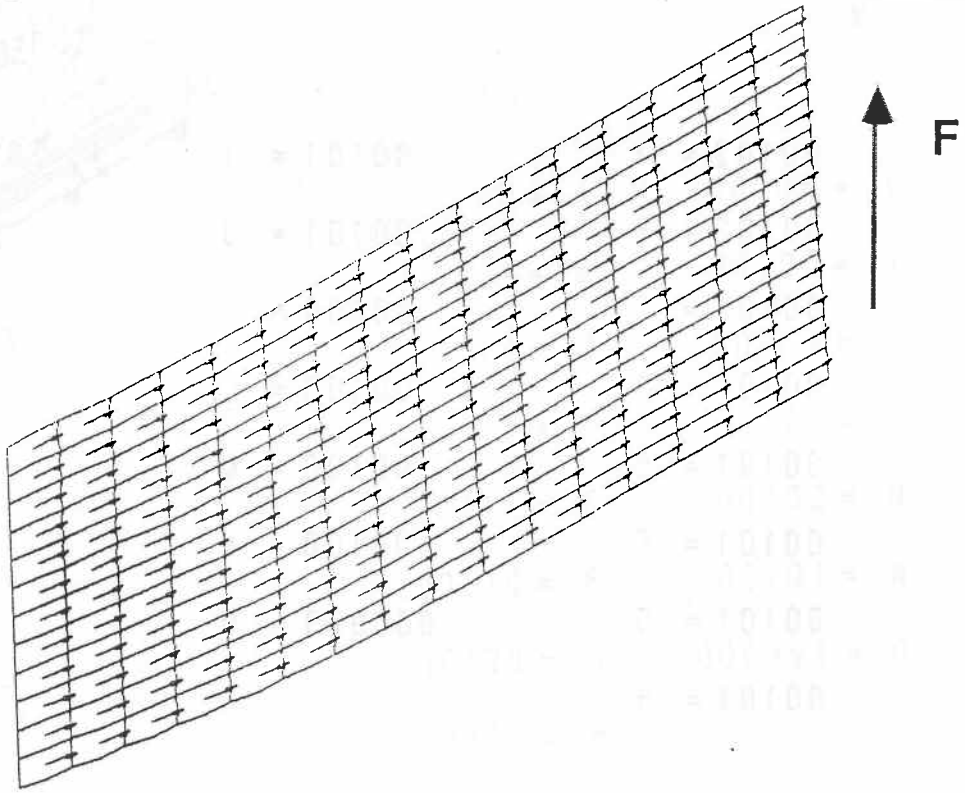

(d)

Figure 3: 0° Cantilever Beam
(d) Updated Geometry and Fiber Orientation After 10 seconds, 20 Time Steps,
(e) Updated Geometry and Fiber Orientation After 15 seconds, 30 Time Steps.

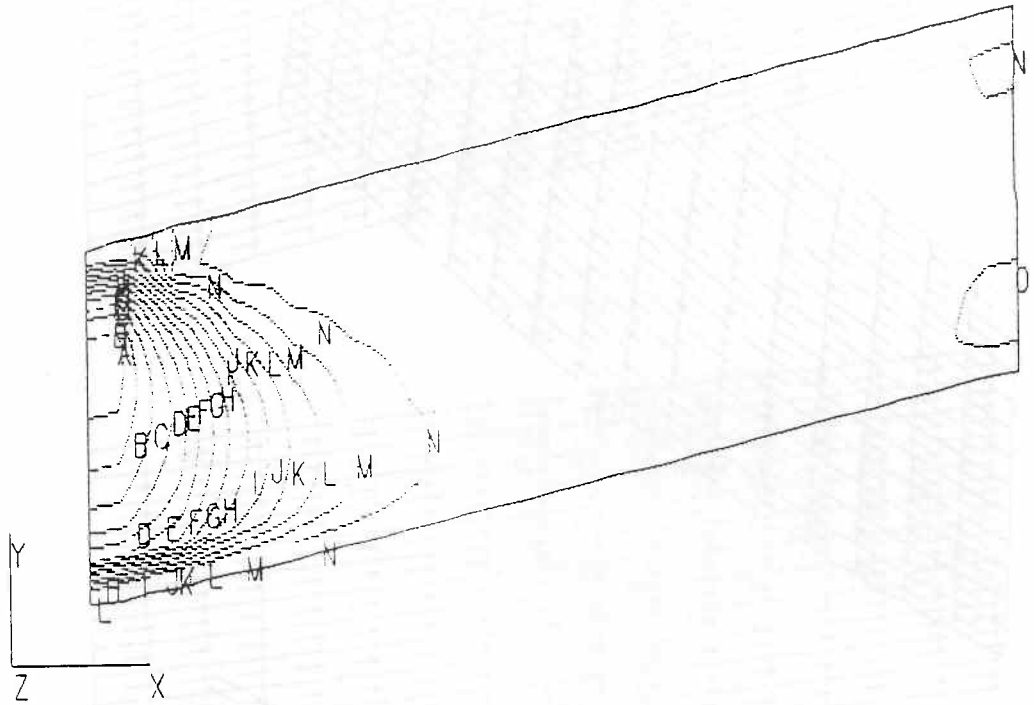

.00102 = A	.00101 = I
.00102 = B	.00101 = J
.00101 = C	.00100 = K
.00101 = D	.00100 = L
.00101 = E	.00100 = M
.00101 = F	.00100 = N
.00101 = G	.000999 = O
.00101 = H	

Figure 5: 0° Cantilever Beam Thickness Contours after 5 Seconds, 10 Time Steps. Original Thickness = 0.001.

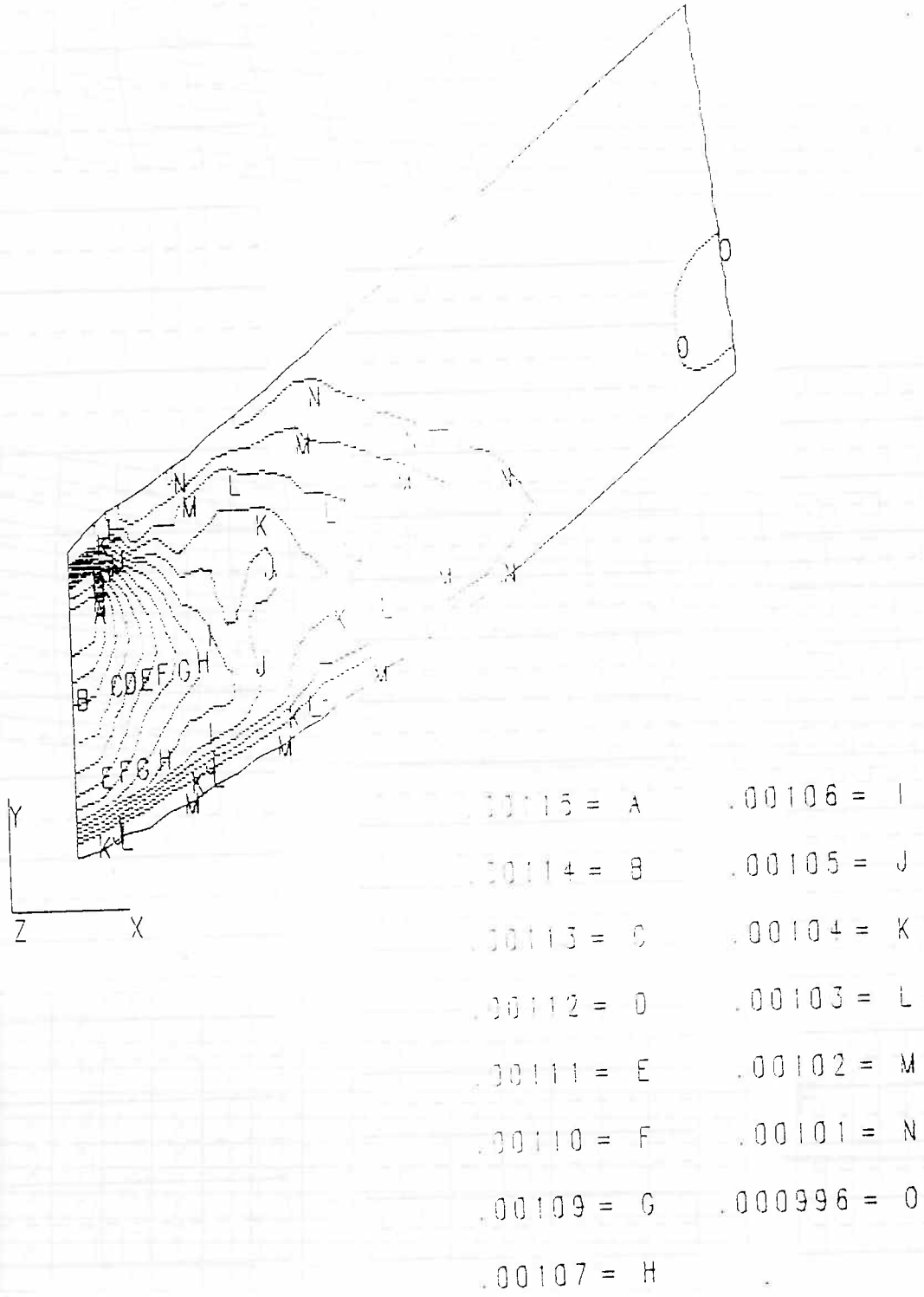

Figure 6: 0° Cantilever Beam Thickness Contours after 15 Seconds, 30 Time Steps. Original Thickness = 0.001.

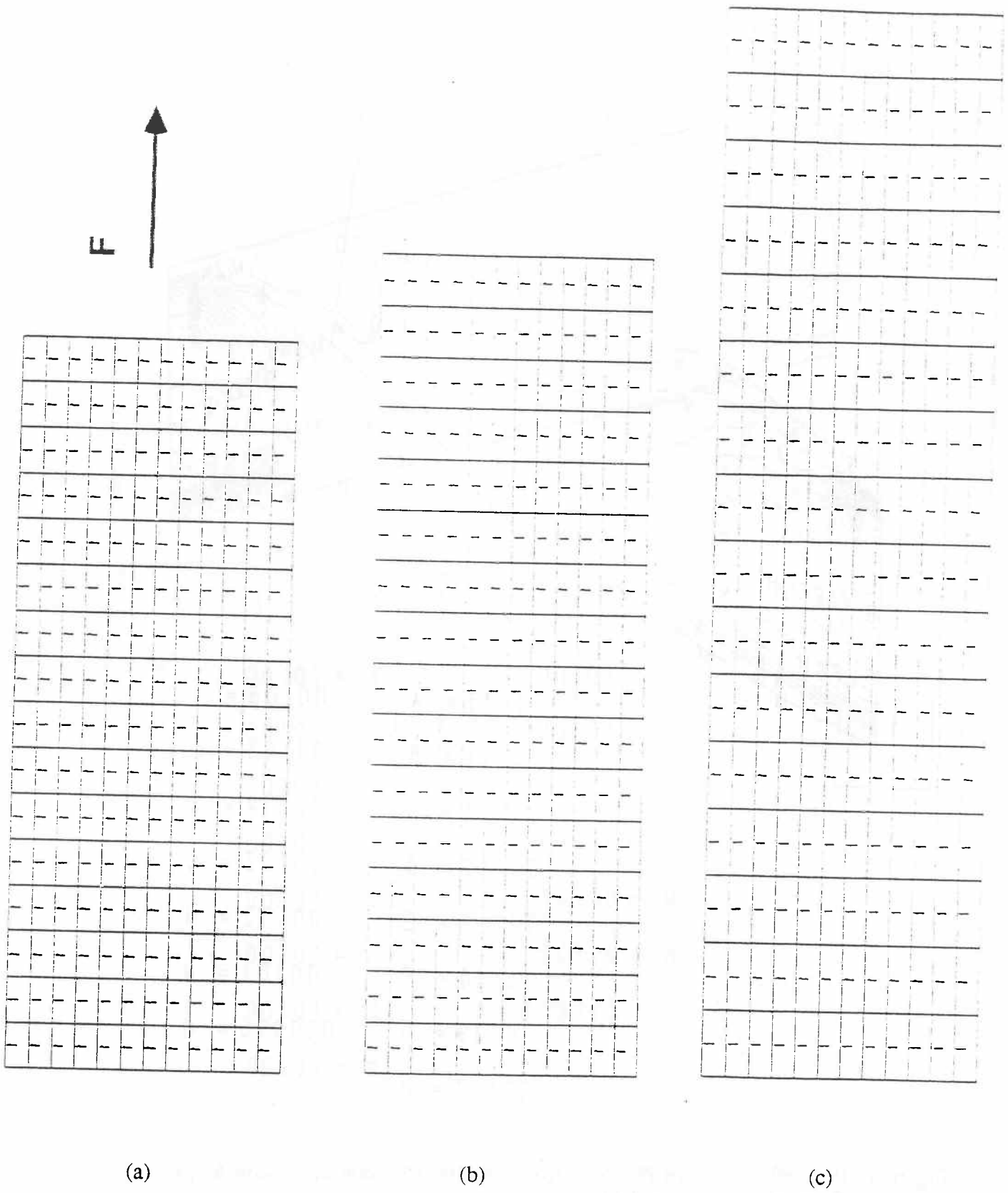

Figure 7: Beam With 90° Fiber Orientation Subject to Uniform Tensile End Loading
(a) Original Position;
(b) Updated Geometry and Fiber Orientation after 5 Seconds, 10 Time Steps;
(c) Updated Geometry and Fiber Orientation after 15 Seconds. 30 Time Steps.

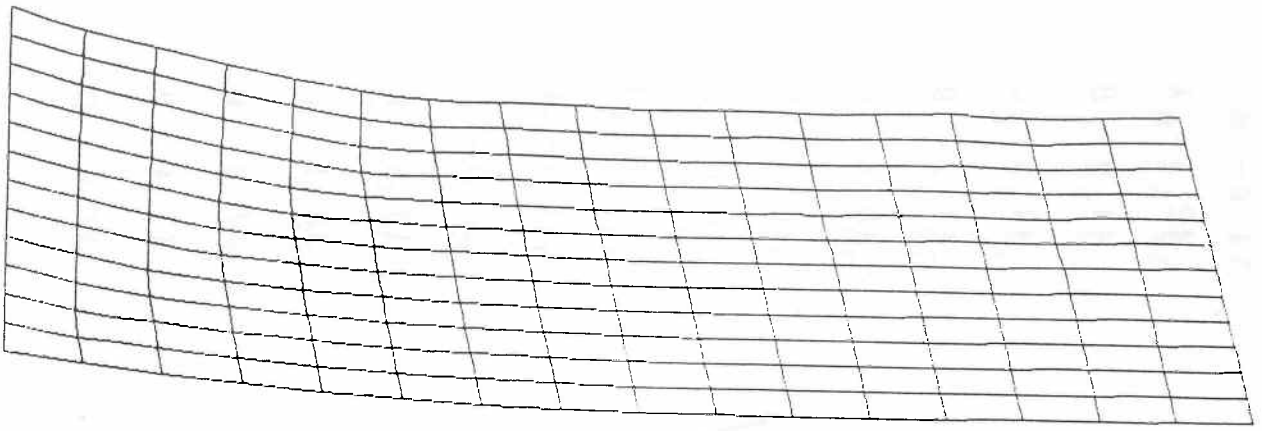

(c)

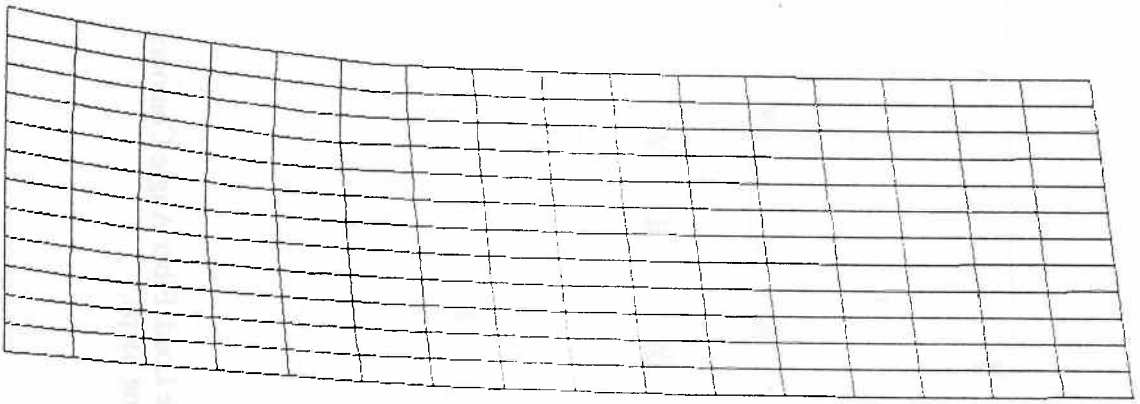

(b)

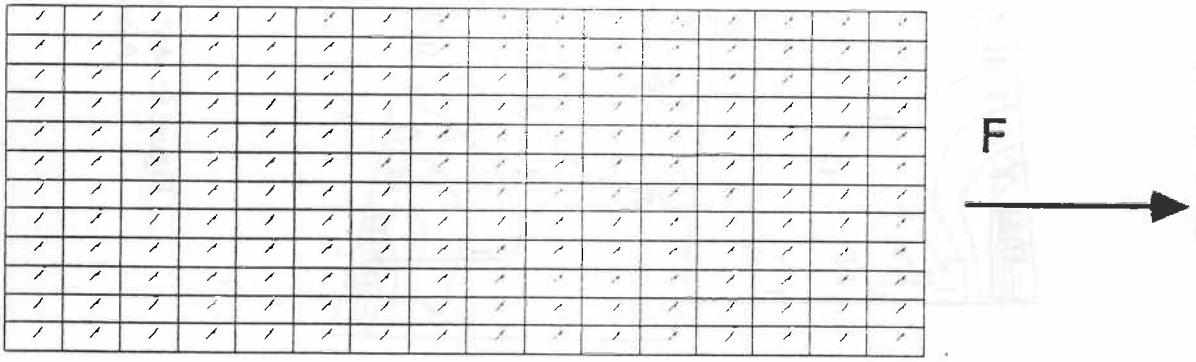

(a)

Figure 8: Beam With 45° Fiber Orientation Subject to Uniform Tensile End Loading
(a) Original Position;
(b) Updated Geometry after 5 Seconds, 10 Time Steps;
(c) Updated Geometry after 15 Seconds, 30 Time Steps.

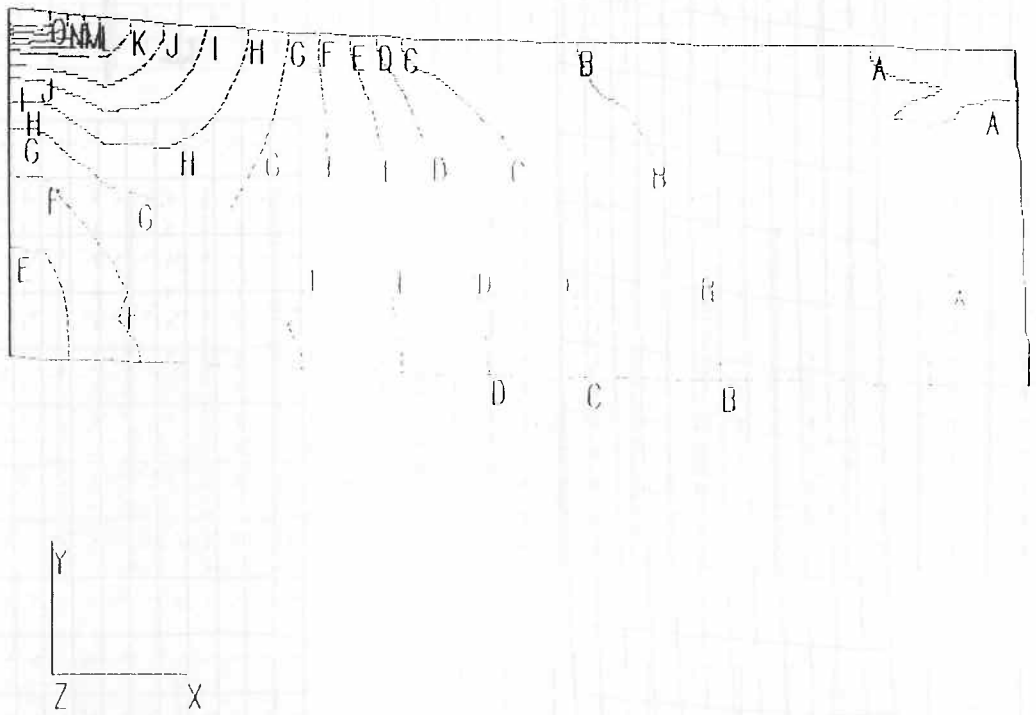

42.3 = A

41.9 = B

41.5 = C

41.2 = D

40.8 = E

40.4 = F

40.0 = G

39.7 = H

39.3 = I

38.9 = J

38.5 = K

38.1 = L

37.8 = M

37.4 = N

37.0 = O

Figure 9: 45° Beam Under Tensile Load. Fiber Angle Contours After 5 Seconds, 10 Time Steps.

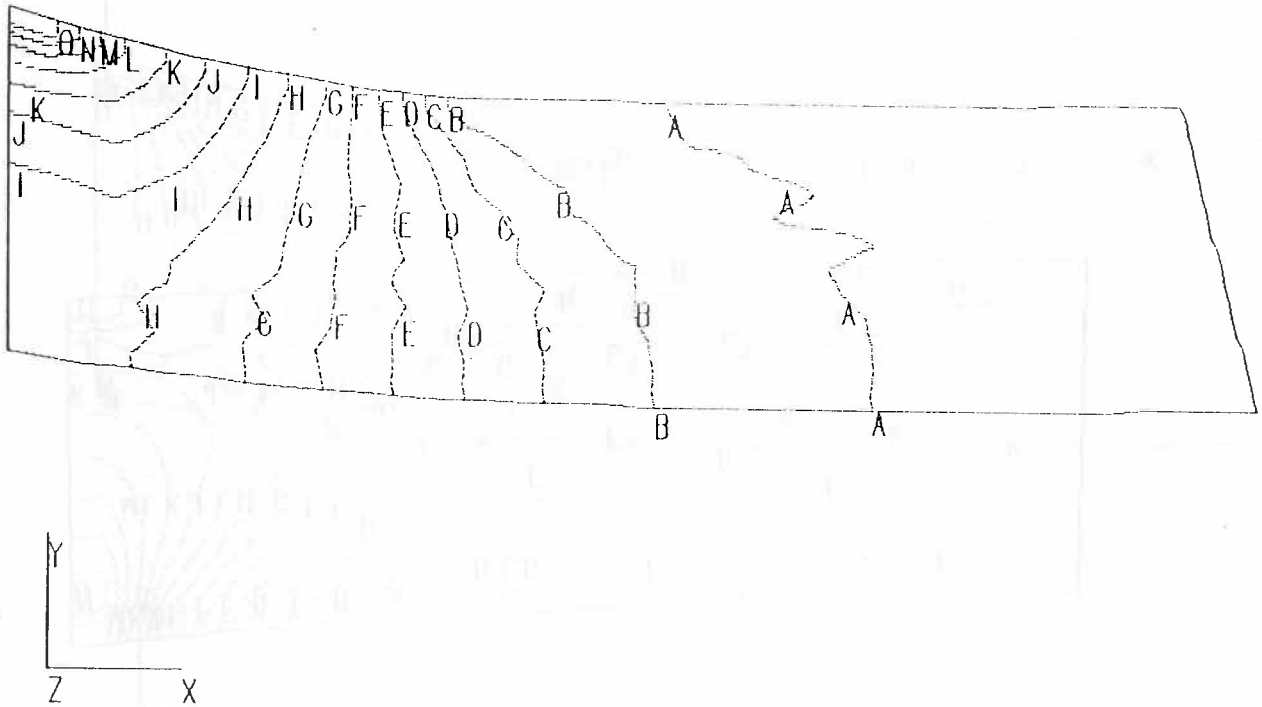

38.8 = A

37.7 = B

36.6 = C

35.5 = D

34.4 = E

33.3 = F

32.2 = G

31.2 = H

30.1 = I

29.0 = J

27.9 = K

26.8 = L

25.7 = M

24.6 = N

23.6 = O

Figure 10: 45° Beam Under Tensile Load. Fiber Angle Contours After 15 Seconds, 30 Time Steps.

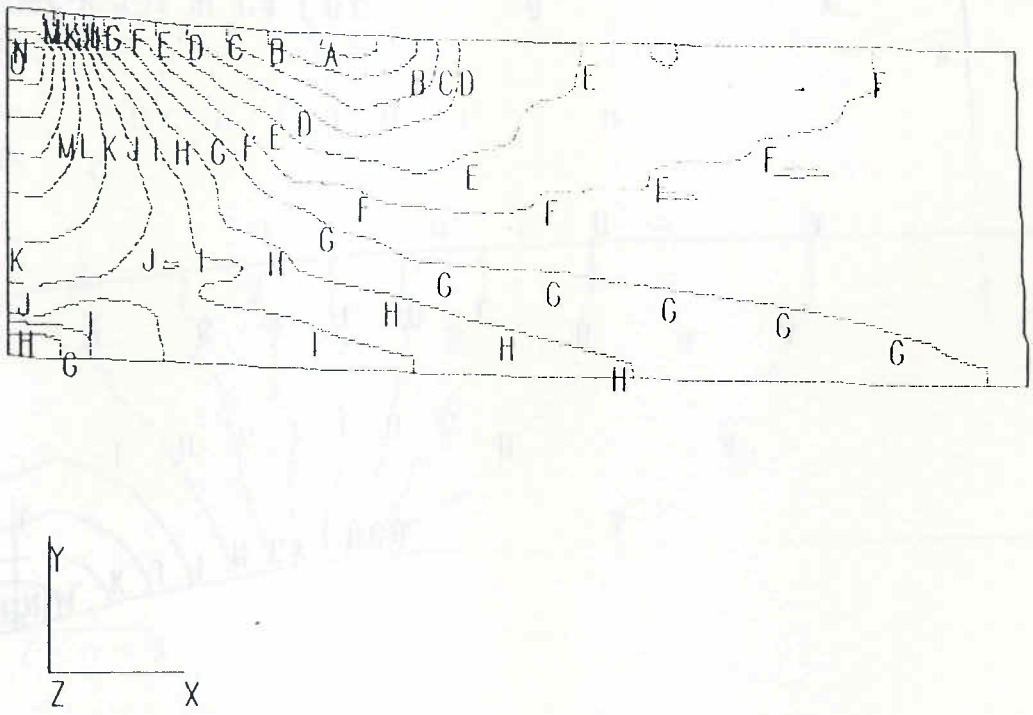

.000963 = A

.000960 = B

.000958 = C

.000955 = D

.000953 = E

.000950 = F

.000947 = G

.000945 = H

.000942 = I

.000939 = J

.000937 = K

.000934 = L

.000931 = M

.000929 = N

.000926 = O

Figure 11: 45° Beam Under Tensile Load. Thickness Contours After 5 Seconds, 10 Time Steps. Original Thickness = 0.001.

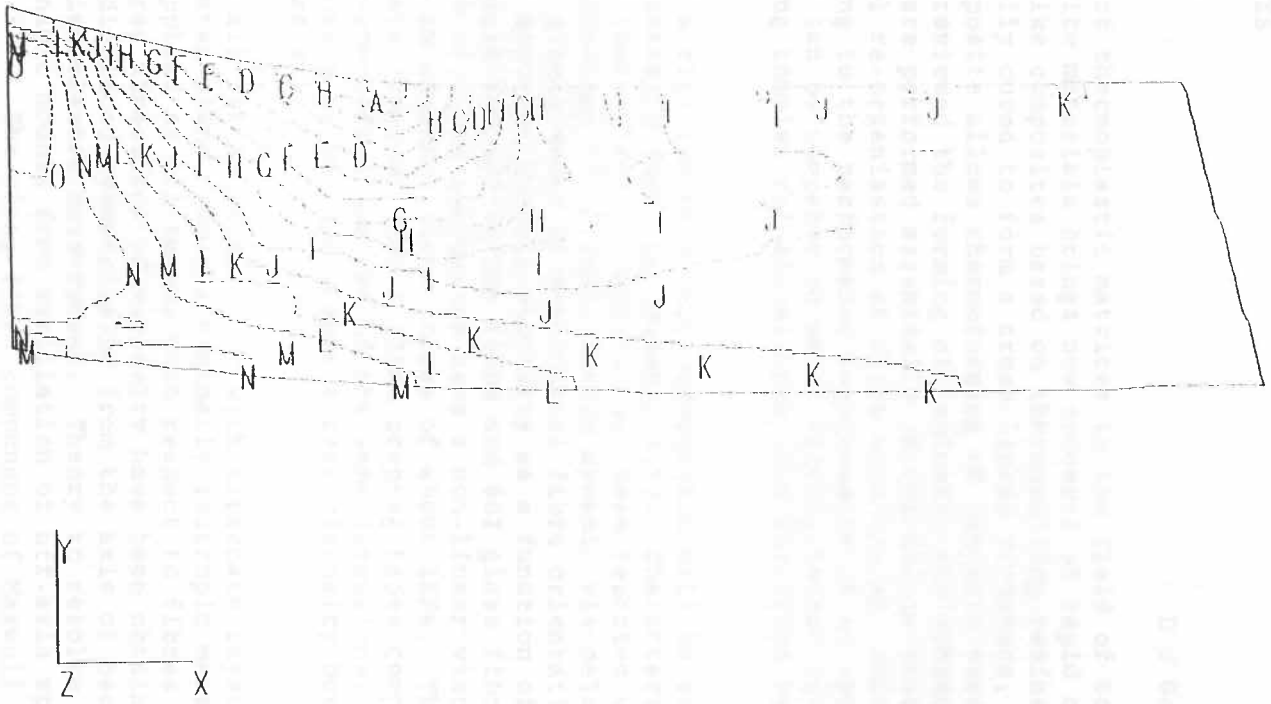

.000907 = A
.000901 = B
.000895 = C
.000889 = D
.000883 = E
.000877 = F
.000871 = G
.000865 = H
.000859 = I
.000853 = J
.000847 = K
.000841 = L
.000835 = M
.000829 = N
.000823 = O

Figure 12: 45° Beam Under Tensile Load. Thickness Contours After 15 Seconds, 30 Time Steps. Original Thickness = 0.001.